Natural Resources Canada
Ressources naturelles Canada

Distinguishing primary and mineralization-related signatures of chert from the banded iron-formation–hosted gold deposits at Musselwhite, Ontario and Meadowbank, Nunavut

B. Gourcerol, P.C. Thurston, D.J. Kontak, O. Côté-Mantha, and J. Biczok

Geological Survey of Canada
Current Research 2015-1

2015

Canada

Geological Survey of Canada
Current Research 2015-1

Distinguishing primary and mineralization-related signatures of chert from the banded iron-formation–hosted gold deposits at Musselwhite, Ontario and Meadowbank, Nunavut

B. Gourcerol, P.C. Thurston, D.J. Kontak, O. Côté-Mantha, and J. Biczok

2015

ISSN 1701-4387
Catalogue No. M44-2015/1E-PDF
ISBN 978-1-100-25346-6
doi:10.4095/295531

A copy of this publication is also available for reference in depository libraries across Canada through access to the Depository Services Program's Web site at http://dsp-psd.pwgsc.gc.ca

This publication is available for free download through GEOSCAN
http://geoscan.ess.nrcan.gc.ca

Recommended citation

Gourcerol, B., Thurston, P.C., Kontak, D.J., Côté-Mantha, O., and Biczok, J., 2015. Distinguishing primary and mineralization-related signatures of chert from the banded iron-formation–hosted gold deposits at Musselwhite, Ontario and Meadowbank, Nunavut; Geological Survey of Canada, Current Research 2015-1, 21 p. doi:10.4095/295531

Critical review

S. Castonguay

Authors

B. Gourcerol (gourcerol.blandine@gmail.com)
P.C. Thurston (pthurston@laurentian.ca)
D.J. Kontak (DKontak@laurentian.ca)
Mineral Exploration Research Centre
Laurentian University
Sudbury, Ontario P3E 2C6

O. Côté-Mantha (olivier.cote-mantha@agnicoeagle.com)
Agnico Eagle Mines Ltd – Division Exploration
765, Chemin de la mine Goldex
Val d'Or, Quebec J9P 4N9

J. Biczok (john.biczok@goldcorp.com)
Goldcorp Canada Ltd.
Musselwhite mine, P.O. Box 7500
Thunder Bay, Ontario P7B 6S8

Correction date:

Distinguishing primary and mineralization-related signatures of chert from the banded iron-formation–hosted gold deposits at Musselwhite, Ontario and Meadowbank, Nunavut

B. Gourcerol, P.C. Thurston, D.J. Kontak, O. Côté-Mantha, and J. Biczok

Gourcerol, B., Thurston, P.C., Kontak, D.J., Côté-Mantha, O., and Biczok, J., 2015. Distinguishing primary and mineralization-related signatures of chert from the banded iron-formation–hosted gold deposits at Musselwhite, Ontario and Meadowbank, Nunavut; Geological Survey of Canada, Current Research 2015-1, 21 p. doi:10.4095/295531

Abstract: Algoma-type banded iron-formation units are generally Archean chemical sedimentary rocks comprised of alternating layers of iron-rich minerals and chert that are stratigraphically associated with submarine volcanic rocks and localized within greenstone belts. Although much research has been done on Algoma-type banded iron-formation units, their depositional and overall geological settings are contentious due to overprinting effects of postdepositional deformation and metamorphism and the absence of modern analogues for comparative studies.

Geochemical study of the gold-hosting Algoma-type banded iron-formation units at the Musselwhite and Meadowbank deposits provide comparable information on their depositional context. Geochemical tools, such as rare-earth element REE+Y systematics, indicate that chert bands in Algoma-type banded iron-formation record contributions from: 1) seawater, characterized by enrichment in HREEs relative to LREEs, and positive La, Gd, and Y anomalies; 2) hydrothermal fluids, characterized by a positive Eu anomaly and a flat pattern; and 3) hydrogeneous contamination. A detailed study of both of the aforementioned deposits was undertaken to evaluate the origin of the chert in these banded iron-formation settings. A hydrothermal overprint on banded iron-formation from the Musselwhite deposit is proposed to explain negative Ce anomalies that may be due to late hydrothermal fluid circulation in the chert bands replacing the initial seawater component. This hydrothermal alteration phase may be associated with the gold mineralization.

Résumé : Les formations de fer rubanées de type Algoma sont généralement des roches sédimentaires d'origine chimique de l'Archéen constituées d'une alternance de minéraux riches en fer et de chert, qui sont stratigraphiquement associé à des roches volcaniques sous-marines et situées dans des ceintures de roches vertes. Bien que beaucoup de recherches ont été effectuées sur les formations de fer de type Algoma, leurs paramètres de dépôt et leurs caractéristiques géologiques d'ensemble prêtent à controverse en raison de la superposition des effets de la déformation postsédimentaire et du métamorphisme, mais également de l'absence d'analogues modernes pour des études comparatives.

L'étude géochimique des formations de fer rubanées de type Algoma minéralisées en or dans les gisements de Musselwhite et de Meadowbank fournit des informations comparables sur le contexte de leur dépôt sédimentaire. Les outils géochimiques, tels que la systématique éléments des terres rares (ÉTR) + Y, indiquent que les bandes de chert dans les formations de fer rubanées de type Algoma enregistrent les contributions des éléments suivants : 1) l'eau de mer, caractérisée par un enrichissement en terres rares lourdes par rapport aux terres rares légères ainsi que des anomalies positives en La, Gd et Y; 2) des fluides hydrothermaux, caractérisés par une anomalie positive en Eu et un spectre plat; et 3) une contamination hydrogénique. Une étude détaillée de chacun des deux gisements mentionnés ci-dessus a été entreprise pour évaluer l'origine du chert dans ces cadres de formations de fer rubanées. Une surimpression hydrothermale de sur ceraines de fer rubanées au gisement de Musselwhite est propsée por expliquer des anomalies négatives en Ce, qui pourraient être associées à la circulation de fluides hydrothermaux tardifs dans les bandes de chert, remplaçant la composante initiale d'eau de mer. Cette phase d'altération hydrothermale pourrait être associée à la minéralisation aurifère.

INTRODUCTION

Algoma-type banded iron-formation units are thinly bedded, chemical sedimentary rocks comprising alternating layers of iron-rich minerals and chert (James, 1954) stratigraphically associated with submarine, volcanic rocks in Eoarchaean to Paleoproterozoic greenstone belts (Goodwin, 1973; Bekker et al., 2010). Studies of gold deposits associated with Algoma-type banded iron-formation in Archaean cratons have shown that gold is associated with localized sulphide-facies zones within regionally extensive oxide-facies units (e.g. Kaapvaal, Zimbabwe, Superior, Slave, and Churchill Province (Phillips et al., 1984; Kerswill, 1993, 1996; Bleeker, 2007; Biczok et al., 2012). The depositional and geological settings of these deposits are contentious due to postdepositional overprinting and the absence of modern analogues. The iron-bearing minerals in iron-formation units precipitated from basin waters and hydrothermal vents; they include siderite and/or iron oxy-hydroxide minerals diagenetically transformed to hematite, magnetite, iron-silicate minerals, and sulphide minerals. The origin of chert is controversial, but the consensus is that it, like the iron-bearing minerals, originated as a seawater precipitate (Bolhar et al., 2005; Thurston et al., 2011) or as a hydrothermal precipitate (Allwood et al., 2010; Thurston et al., 2011), or by replacement (Hanor and Duchac, 1990). Because of the possibility of alteration during diagenesis, the present authors examine the geochemistry of chert beds in that they more likely preserve their original chemistry.

In regard to banded iron-formation–hosted gold deposits, do the gold mineralizing fluids prefer one geochemical type of iron-formation versus another? Lode-gold and banded iron-formation–hosted gold deposits are widely conceded to be epigenetic (Goldfarb et al., 2001, 2005), thus, at a regional scale the geochemical signature of the chert component of banded iron-formation units may provide a vector toward zones with an enhanced potential to host gold mineralization. Consequently, a study of the geochemical characteristics of Algoma-type banded iron-formation, both barren and those associated with gold mineralization, may address important issues regarding these deposits by: 1) providing insights on which type of iron-formation makes a better host for gold mineralization by identifying and using the pre-mineralized chemical signal; 2) allowing a better understanding of the mineralizing processes; 3) providing a geochemical footprint of the mineralized system; and 4) collectively providing a vectoring tool from least or unaltered to altered mineralized zones.

This paper presents the results of in situ laser ablation inductively coupled mass spectrometric (LA ICP-MS) analysis of chert from banded iron-formation–hosted lode-gold deposits in the Superior and Churchill cratons, namely: 1) the Musselwhite deposit (11.23 Mt proven and/or probable grading 6.34 g/t gold in 2011), in the North Caribou greenstone belt of the Superior Province (Biczok et al., 2012); and 2) the Meadowbank deposit (24.5 Mt proven and/or probable ore reserve at 2.8 g/t in 2011), located in the Woodburn Lake Group of the Rae Domain (Churchill Province).

GEOLOGICAL SETTING

Superior Province

The Archean Superior Province consists of east-trending continental fragments interspersed with linear metasedimentary basins (Percival, 2007). The 3–2.9 Ga North Caribou Superterrane was divided into multiple domains and terranes (Thurston et al., 1991). The North Caribou Superterrane comprises granitoid basement (Thurston et al., 1991; Percival, 2007) and overlying volcanic belts (e.g. North Caribou greenstone belt) all cratonized at ca. 2.87 Ga (Stott et al., 1989).

The North Caribou greenstone belt lies at the northern boundary of the North Caribou Terrane (Biczok et al., 2012). This greenstone belt comprises a core of metasedimentary rocks flanked by metavolcanic units; all subdivided into eight supracrustal assemblages (Fig. 1) (Breaks et al., 2001). Recent geochronological work (Biczok et al., 2012; McNicoll et al., 2013) dated the units of the greenstone belt between 2980 Ma and 2856 Ma. These results also indicate that the Opapimiskan Lake package in the vicinity of the Musselwhite mine is overturned (McNicoll et al., 2013) and likely thrust over the younger metasedimentary rocks. Further complicating the picture is the recent discovery of volcanic units immediately south of the mine dated at ca. 2863 Ma and 2734 Ma (V. McNicoll, pers. comm., 2013). Similar banded iron-formation units are found in at least three of the volcanic units of very different ages and it is hoped that this study will help distinguish these various banded iron-formation units. The belt is bounded by metamorphosed felsic plutonic rocks, in particular the ca. 2.87 Ga North Caribou Lake batholith and the Schade Lake gneissic complex (ca. 2857–2856 Ma; DeKemp (1987); Biczok et al. (2012)).

Musselwhite deposit

Located in the North Caribou greenstone belt (Fig. 1), the Musselwhite mine is a world-class deposit with past production and current reserves and resources totalling 5.41 million ounces (153.3 t) (Biczok et al., 2012). The lithostratigraphy is dominated by banded iron-formation units and mafic to ultramafic metavolcanic rocks of the Opapimiskan-Markop metavolcanic assemblage dated between 2973 Ma and 2967 Ma plus tholeiitic basalt and minor felsic volcanic rocks of the 2982–2980 Ma South Rim metavolcanic assemblage (Biczok et al., 2012; McNicoll et al., 2013). Recent geochronology and field mapping indicate that the mine stratigraphy is overturned (McNicoll et al., 2013). The deposit itself is composed of multiple ore bodies hosted by two main iron-formation units within the Opapimiskan Lake metavolcanic assemblage.

The Opapimiskan-Markop metavolcanic assemblage is composed, from the structural base to the top, of the 'lower basalt' unit, the 'southern iron-formation', 'basement basalt' unit, and the 'northern iron-formation'. The South Rim metavolcanic assemblage is composed, from base to top, of metamorphosed mafic volcaniclastic and flow units named the Bvol unit, and by dacitic to rhyolitic rocks named the Avol unit (Otto, 2002; Moran, 2008; Biczok et al., 2012).

The north iron-formation, the main host to mineralization, is subdivided, from the structural base to top, into: pyrrhotite-rich mudstone (unit 4H), chert-grunerite (unit 4A), chert-magnetite (unit 4B), clastic-chert-magnetite ('clastic' unit 4B), garnet-grunerite-chert (unit 4EA), garnetiferous amphibolite (unit 4E), and garnet-biotite schist (unit 4F) (Otto, 2002; Moran, 2008; Biczok et al., 2012, Oswald et al., 2014). The main mineralized horizons are the 4EA and 4B units. The southern iron-formation consists of two subparallel banded iron-formation horizons only locally mineralized (Biczok et al., 2012).

The basement basalt unit lying between the northern and southern iron-formations is a thick sequence of massive- and pillowed tholeiitic basalt (Moran, 2008). The lower basalt unit is the structural footwall (Otto, 2002) and is composed of basalt and ultramafic rocks, but includes extensive andesite (Hollings and Kerrich, 1999). The presence of pillow structures suggests a submarine environment (Otto, 2002; Moran, 2008).

Deformation

Three deformation events were recognized in the North Caribou greenstone belt (Hall and Rigg, 1986; Breaks et al., 2001; Oswald et al., 2014). The first deformation (D_1) is seen in tight F_1 folds up to several metres long with a well developed S_1 fabric in schistose ultramafic units, and the property-scale repetition of units (Oswald et al., 2014). The second deformation (D_2) is the most important structural fabric, which produced a moderate to strong, subvertical

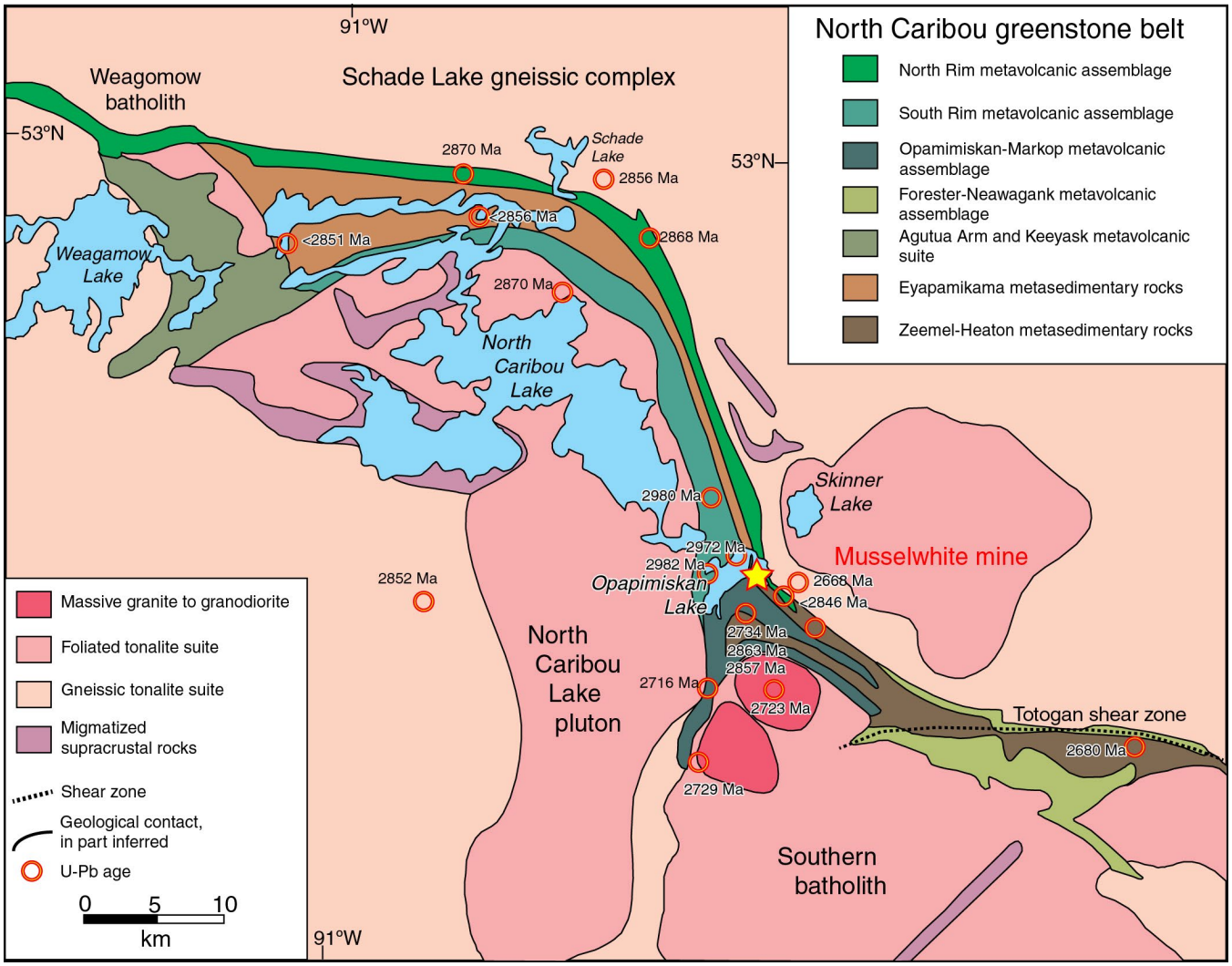

Figure 1. Geological map of the Musselwhite deposit area (*modified from* Biczok et al., 2012).

north-trending S_2 foliation axial-planar to mesoscopic F_2 folds (Breaks et al., 2001). The third deformation (D_3) is relatively weak and is recognized by a crenulation cleavage overprinting D_2 in grunerite-rich banded iron-formation.

Metamorphism

Regional metamorphism of the North Caribou greenstone belt varies from lower greenschist to low-mid amphibolite facies (Breaks et al., 2001). The Musselwhite area is affected by two events, one middle amphibolite prograde (>600°C) and the other a chlorite retrograde (210°C to 250°C) (Otto, 2002; Isaac, 2008).

Mineralization

Mineralization consists of epigenetic gold associated with high-strain zones mainly along the steep limbs of the folded iron-formation (Biczok et al., 2012, Oswald et al., 2014). Gold mineralization developed under amphibolite conditions (i.e. 540°C to 600°C) (Otto, 2002).

The most important host of gold mineralization in the Musselwhite deposit is the silicate-facies iron-formation (unit 4EA) composed mainly of grunerite-garnet interlayered with chert (Biczok et al., 2012). Garnet crystals in barren unit 4EA are anhedral to suhedral, medium grained, and contain numerous inclusions of grunerite and other silicate minerals. The continuation of strain after the formation of brittle hydrothermal garnet crystals within the relatively more ductile grunerite matrix led to the development of extensive fractures in the garnet crystals, as well as pressure shadows, into which pyrrhotite and gold were deposited (Kolb, 2010; Biczok et al., 2012). Retrograde phases such as chlorite were developed locally (Otto, 2002). The 4B unit consists of finely laminated layers of quartz and magnetite, with minor grunerite. The typical 'pure' unit 4B is relatively unaltered adjacent to any mineralized zone compared to unit 4EA. Mineralized unit 4B is cut by quartz±pyrrhotite veins and may develop grunerite replacement of the quartz-magnetite layers. The 'clastic' variety of unit 4B contains diffuse layers of very fine-grained chert, magnetite, and amphibole±garnet. In the vicinity of the high-strain zones on the limbs of the F_2 folds, these silicate layers are prone to replacement by hydrothermal biotite and garnet±green amphibole (Otto, 2002).

Churchill Province

The Archean Churchill Province has been subdivided into the Hearne and Rae domains, (Hoffman, 1989). The Rae Domain consists of the ca. 2.7 Ga Woodburn Lake Group (Ashton, 1985; Roddick et al., 1992; Aspler and Chiarenzelli, 1996) and the ca. 2.9 Ga Prince Albert Group (Schau, 1982; Aspler and Chiarenzelli, 1996), which includes granitoid and mafic-ultramafic volcanic rocks, iron-formation, shallow-water quartz arenite and minor felsic volcanic rocks (Miller and Tella, 1995). Aspler and Chiarenzelli (1996) proposed the quartzite and komatiite of the Rae Domain were deposited during extension of "Nunavutia" a basement block (Pehrsson et al., 2013) that was later overlain by volcanic rocks of a back-arc sequence or an arc-trench system.

The Hearne Domain is a granite-greenstone terrane composed of multicyclic, mafic to felsic volcanic rocks intercalated with immature sandstone, pelite, and iron-formation with rare quartz arenite and spinifex-textured ultramafic rocks (Miller and Tella, 1995; Aspler and Chiarenzelli, 1996).

Meadowbank deposit

The Meadowbank deposit in the Rae Domain is contained within the Woodburn Lake Group (ca. 2.71 Ga), consisting of tholeiitic and komatiitic metavolcanic rocks with minor calc-alkaline felsic tuffs and flows with intercalated iron-formation and clastic metasedimentary rocks (Armitage et al., 1996; Sherlock et al., 2001a, b, 2004; Hrabi et al., 2003; Pehrrson and Wilkinson, 2004). All of these units are intruded by mafic and felsic plutonic rocks.

The Meadowbank area (Fig. 2) contains two main gold deposits: the Meadowbank mine and the Vault deposit. The Meadowbank mine is mainly hosted within strongly altered and deformed, sulphide-bearing portions of the Central banded iron-formation (Sherlock et al., 2001a; Hrabi et al., 2003; Sherlock et al., 2004), whereas the Vault deposit is hosted by sericite-chlorite-pyrite and carbonate-altered intermediate to felsic volcanic rocks (Hrabi et al., 2003; Sherlock et al., 2004).

Numerous units of Algoma-type banded iron-formation, 0.2–10 m thick, have been identified. These banded iron-formation units include the 'Far West' 'BIF', West IF, 'Central BIF', 'East BIF', and 'Grizzly', all generally interlayered with the volcanic rocks and locally with a quartzite unit (Fig. 2; Sherlock et al., 2001a, b, 2004; Gourcerol et al., 2014). These banded iron-formation units are described more in detail in Gourcerol et al. (2014).

Deformation

The structural setting of the Meadowbank area is complex, consisting of six regional-scale ductile deformation events spanning the Neoarchean to Paleoproterozoic (e.g. Ashton, 1985; Henderson et al., 1991; Pehrsson et al., 2013). The D_1 and D_2 events had a significant effect on the geometry of the mineralized bodies in the Third Portage area (Ashton, 1985; Sherlock et al., 2004; Janvier et al., 2013). Some relict bedding (S_0) is preserved in the quartz arenite and in the iron-formation (Armitage et al., 1996). D_2 represents the main structural event in the Meadowbank area (Janvier et al., 2013).

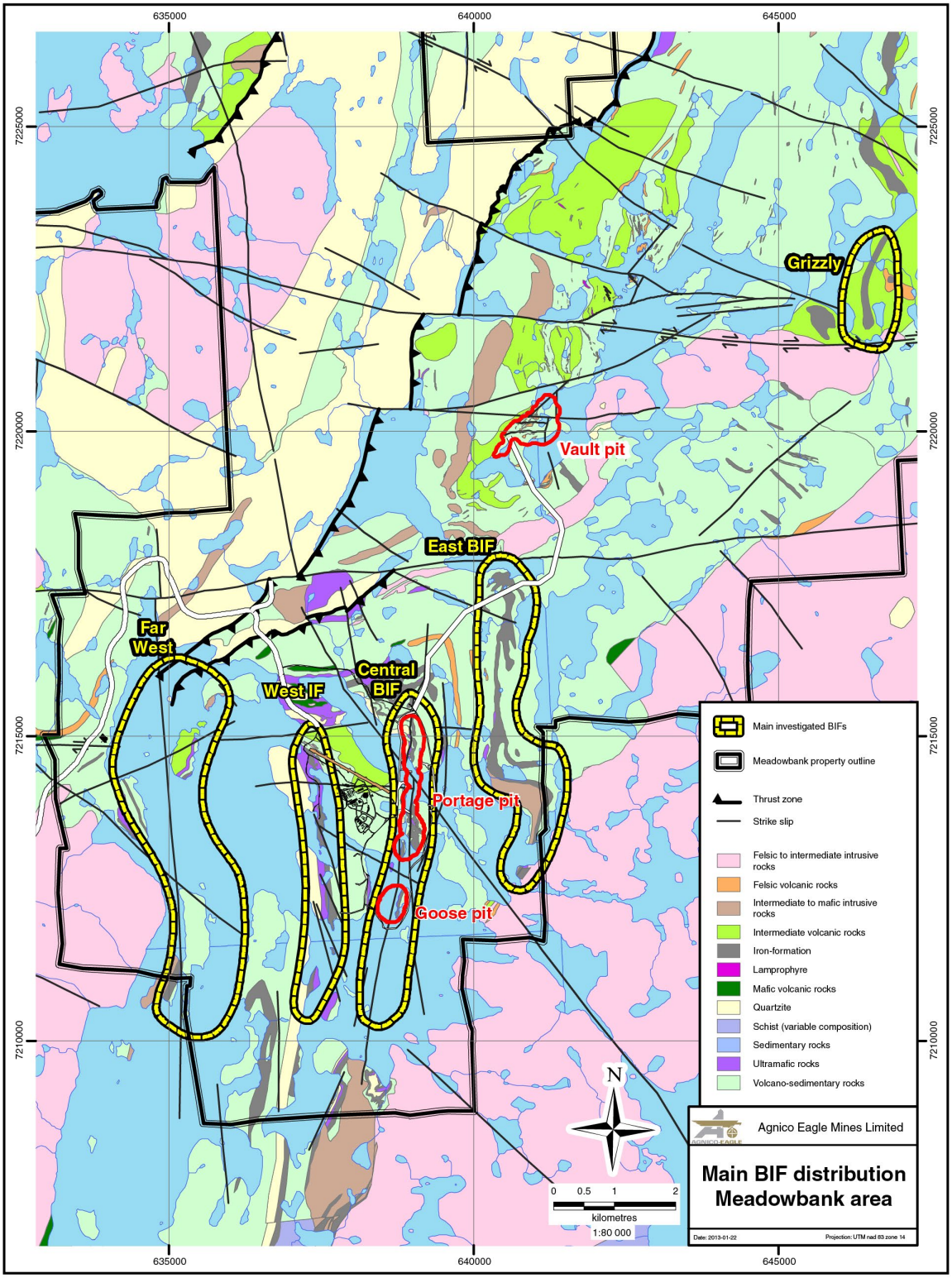

Figure 2. Geological map of the Meadowbank deposit area showing the location of the main banded iron-formation (BIF) units that have been sampled for this study (*modified from* O. Côté-Mantha, unpub. company report for Agnico Eagle Mine Ltd., 2012).

Metamorphism

Three distinct regional metamorphic events are recognized in the Meadowbank area. The M_1 is a greenschist-grade event dated at less than 2.60 Ga to more than 1.8–1.9 Ga. The M_2 varies across the property from a mid-greenschist to amphibolite grade. This event is dated coeval with D_2. The M_3 shows a mid-upper greenschist to amphibolite grade, characterized by a new generation of biotite, garnet, cummingtonite, and actinolite and is dated as postmineralization (ca. 1.8 Ga).

Mineralization

Five principal mineralized zones are defined (Armitage et al., 1996; Davis and Zaleski, 1998; Pehrsson et al., 2000; Sherlock et al., 2001a, b; Hrabi et al., 2003; Pehrsson and Wilkinson, 2004) and these are: Vault, North Portage, Third Portage, Bay Zone, and Goose Island (Fig. 2).

The orebodies of the Meadowbank mine in the Central banded iron-formation consist of several subparallel bands of auriferous iron-formation. Sherlock et al. (2001a, b) suggested that the orebodies are mostly developed at the contact between an ultramafic body and the volcano-sedimentary package. According to Armitage et al. (1996) and Sherlock et al. (2001a, b), epigenetic gold mineralization is closely associated with D_1-D_2 deformation and originated from the circulation of fluids enriched in Mg, K, Ca, S, As, Cu, and Au (Janvier et al., 2013).

ANALYTICAL METHODS AND DATA TREATMENT

Twenty-three samples of iron-formation from drill core and outcrop were collected from the Musselwhite deposit (i.e. chert-magnetite (unit 4B), garnet-grunerite-(chert) (unit 4EA), garnetiferous amphibolite (unit 4E), and garnet-biotite schist (unit 4F)), and thirty-nine from the Meadowbank deposit (i.e. the Far West, West IF, Central BIF, East BIF, and Grizzly). These samples were selected for petrographic study with an emphasis on the chert or chert-carbonate phases. An effort was made to avoid banded iron-formation with chert bands less than 0.05 cm thick since analysis of such thin bands presents challenges. In addition, chert bands were analyzed in preference to Fe-rich bands to minimize the effects of any diagenetic alteration. Polished thin sections from these samples were examined in detail, using both transmitted and reflected light microscopy followed by SEM-EDS imaging and analysis.

Trace-element and REE chemistry was obtained on 100 µm thick polished sections following petrographic study. Based on the REE chemistry observations, areas for analysis were selected to minimize the presence of phases other than silica replacing chert, alteration, and mineral inclusions. Analyses were made using a Resonetics Resolution™ M-50 laser ablation instrument coupled to a Thermo X-Series II quadrupole ICP-MS at the Geochemical Fingerprinting Laboratory of Laurentian University, in Sudbury, Ontario, using the protocol of Kamber and Webb (2007). Line traverses were made on the preselected areas using 140 µm and 190 µm beam diameters with a repetition rate of 10 Hz and an energy density of 7 J/cm^2. The elemental concentrations reported herein represent, therefore, the integrated signal over the length of the traverse. The element list used for each analysis included the 14 REEs in addition to Li, Be, Si, Sc, Ti, V, Cr, Mn, Fe, Co, Ni, Cu, Zn, Ga, As, Rb, Sr, Zr, Nb, Mo, Ag, Cd, In, Sn, Sb, Cs, Ba, Hf, Ta, W, W, Tl, Pb, Th, and U. Silica was used as the internal standard and the NIST 612 glass standard was analyzed at the beginning and at the end of each line traverse. The final concentrations were determined by integration of the signals over the selected length of the traverse.

Only data from samples where all the REEs were above the detection limit are discussed below. In addition, the Queensland (MUQ) shale standard was used for normalizing the REE+Y values. This shale standard is commonly used for normalization of Archean banded iron-formation data due to its dominantly mafic volcanic provenance that is similar to the expected average terrigenous input into the ocean from weathering of upper continental crust (e.g. Bolhar et al., 2005; Thurston et al., 2011). Furthermore, where discussed below, La, Ce, Eu, and Gd anomalies are calculated following the procedure of Lawrence and Kamber (2006) and Pr using the procedure of Bau and Dulski (1996):

$$(La/La)^*_{MUQ} = La/(Pr_{MUQ}*(Pr_{MUQ}/Nd_{MUQ})^2) \quad (1)$$

$$(Ce/Ce)^*_{MUQ} = Ce/(Pr_{MUQ}*(Pr_{MUQ}/Nd_{MUQ})) \quad (2)$$

$$(Pr/Pr)^*_{MUQ} = Pr/(0.5Ce_{MUQ}+0.5Nd_{MUQ}) \quad (3)$$

$$(Eu/Eu)^*_{MUQ} = Eu/(Sm_{MUQ}{}^2*Tb_{MUQ})^{1/3} \quad (4)$$

$$(Gd/Gd)^*_{MUQ} = Gd/(Tb_{MUQ}{}^2*Sm_{MUQ})^{1/3} \quad (5)$$

$$(Lu/Lu)^*_{MUQ} = Lu/(Yb_{MUQ}*(Yb_{MUQ}/Tm_{MUQ})) \quad (6)$$

REVIEW OF REE+Y SYSTEMATICS IN BANDED IRON-FORMATION

The abundance of REE+Y in chert is controlled by three possible processes: 1) precipitation from open-marine seawater (e.g. Bau and Dulski, 1996); 2) precipitation from hydrothermal (i.e. vent sourced) fluids (e.g. Danielson et al., 1992; Allwood et al., 2010); and 3) replacement (e.g. Hanor and Duchac, 1990). All of these processes can be influenced by terrigenous input (Alexander et al., 2008) and oceanographic processes, such as phosphate precipitation. It is customary to normalize samples using a shale standard to minimize the influence of terrigenous input. Yttrium is a rare-earth element with a valence of 3^+, though not a lanthanide, thus it is inserted into the conventional rare-earth element diagram between Dy and Ho, based on its

geochemical behaviour. Given the large beam size used for the analysis, if other phases were present, they would affect the REE+Y pattern and values for elements such as Ga (i.e. clay mineral contamination), Zr (felsic ash contamination), and Th/U (phosphate contamination). In a modern setting, the shale-normalized REE+Y pattern for material precipitated from seawater shows:

1) Depletion in light rare-earth elements (LREEs) relative to heavy rare-earth elements (HREEs);
2) A strongly super-chondritic Y/Ho ratio (i.e. >27), which produces a positive Y anomaly that is often between 40–90;
3) A slightly positive La anomaly (La/La^*_{MUQ} between 1.15 and 1.3);
4) A positive Gd anomaly (Gd/Gd^*_{MUQ} between 1.3 and 1.5);
5) A well developed, negative Ce anomaly resulting from the oxidation of Ce^{+3} to Ce^{+4} in the water column;
6) A minor positive Lu anomaly where analysis of Lu at an appropriate level is available.

Due to the anoxic character of Archean seawater, the shale-normalized REE+Y patterns for Archean seawater is very similar to modern seawater except that Ce shows a negative anomaly (Planavsky et al., 2010).

Based on the above criteria, samples with an Archean seawater pattern should be characterized by the following in shale-normalized REE+Y plots:

1) Depletion in LREEs relative to middle (MREEs) and HREEs;
2) A strongly super-chondritic Y/Ho ratio between 50 and 65;
3) Positive La and Gd anomalies (0.3 to 0.5 and 0.15 to 0.3, respectively);
4) Variable, but well developed positive Eu anomalies (Kamber et al., 2004).

Positive La, Y, and Gd anomalies indicate precipitation from seawater under anoxic conditions (absence of a negative Ce anomaly) with the presence of a positive Eu anomaly, indicating the influence of high-temperature (>250°C) hydrothermal fluids (Bau and Dulski, 1996; Kamber et al., 2004).

Hydrothermal precipitates are characterized by the lack of LREE depletion, absence of both La and Gd anomalies, and the presence of a variably developed Eu anomaly. Crustal contamination may include mineral phases, such as phosphate minerals, clay minerals, and/or resistant minerals (e.g. zircon, xenotime, etc.), all of which induce cause a range of effects upon the REE+Y patterns depending on their modal abundances.

RESULTS

Musselwhite deposit

Samples from the chert-magnetite (unit 4B), garnet-grunerite-(chert) (unit 4EA), garnetiferous amphibolite (unit 4E), and garnet-biotite schist (unit 4F) were normalized to Queensland shale standard (MUQ) (Table 1, 2, 3; Fig. 3a, 4a, 5a, 6a).

The REE+Y normalized data for the unit 4B, 4EA, and 4E samples show, with some minor exceptions, relatively uniform patterns. The data include a moderate enrichment in the HREEs relative to both the LREEs and the MREEs, and La, Gd, and Eu positive anomalies (Table 1, 2, 3) (Fig. 3a, 4a, 5a, 6a). The garnet-biotite schist (unit 4F) facies samples illustrate, however, a different pattern signature and very slightly positive to no Eu anomaly (Fig. 6a). Due to the low concentrations of the REE+Y, the Y/Ho ratios of samples are weakly positive (i.e. chondritic values) and are carefully used in this study.

The chert-magnetite (unit 4B) facies (Fig. 3) shows moderate enrichment in the HREEs relative to both the MREEs and the LREEs (Nd/Yb_{MUQ} = 0.04–0.67), and positive La, Gd, and Eu anomalies (La/La^*_{MUQ} = 1.5–2.6, Gd/Gd^*_{MUQ} = 0.9–1.2, and Eu/Eu^*_{MUQ} = 1.7–3.5) (Table 1). Samples E599668 and E599655 (Fig. 5a) show, however, stronger enrichment in the MREEs relative to LREEs (Pr/Sm_{MUQ} = 0.12–0.36 (Fig. 3a) relative to the majority of samples. The chert-magnetite facies illustrates, therefore, both a seawater and hydrothermal component. To understand the difference in the ∑REE of the patterns, Pr/Sm_{MUQ} ratios and the Sr, Mn, and Ga contents are plotted in Figures 3b, c, and d. The elevated Sr and Mn values (Fig. 3c, b, respectively) suggest samples E599668 and E599655 may be influenced by a source having enrichment in Mn and also to some extent Sr (i.e. proxy of calcium). Observations made with the SEM-EDS confirmed the presence of iron-amphibole minerals (grunerite-cummingtonite), but also the occurrence of calcium-rich amphibole minerals (actinolite) and iron-carbonate around the line traverse and overprinting the chert that could explain the higher concentrations of both Mn and Sr in these samples.

The data for the garnet-grunerite-(chert) (unit 4EA) (Fig. 4) indicate the samples can be subdivided into two distinct groups:

1) Samples E599660, E599662, E599663, E599665, and E599666 show enrichment in the HREEs relative to both the MREEs and the LREEs (Nd/Yb_{MUQ} = 0.15–0.46), and negative La, Gd, and strong positive Eu anomalies (La/La^*_{MUQ} = 0.02–0.51, Gd/Gd^*_{MUQ} = 0.3–0.8, and Eu/Eu^*_{MUQ} = 2.1–3.48) (Table 2).

2) Samples E599654, E599659, and E599667 show variable enrichment in the HREEs relative to both the MREEs and the LREEs (Nd/Yb_{MUQ} = 0.6–2.97), and positive La, Gd, and Eu anomalies (La/La^*_{MUQ} = 1.5-3.02, Gd/Gd^*_{MUQ} = 0.94–1.2, and Eu/Eu^*_{MUQ} = 2.3-3.9) (Table 2).

The first group reflects a strong hydrothermal component without the presence of seawater input and the second group reflects a hydrothermal and seawater combination for the formation of chert. Based on Pr/Sm_{MUQ} ratios and the Mn, Ga, and Sr content, these data suggest sample E599667 may be influenced by a source enriched in Mn, Sr, and Ca (Fig. 4). Enrichment of these elements could be explained by the presence of iron-rich (i.e. grunerite-cummngtonite) and aluminum- and calcium-rich (actinolite) (due to high correlation between the two elements) amphibole minerals occurring as inclusions in the chert and around the line traverse as was also suggested for the chert-magnetite facies.

The garnetiferous amphibolite (unit 4E) facies (Fig. 5) shows enrichment in the HREEs relative to both the MREEs and the LREEs (Nd/Yb_{MUQ} = 0.16–0.71), and variably developed positive La, Gd, and Eu anomalies (La/La^*_{MUQ} = 0.71–1.6, Gd/Gd^*_{MUQ} = 0.92–1.05, and Eu/Eu^*_{MUQ} = 2.42–2.59) (Table 3). For this facies, both a seawater and hydrothermal contribution are suggested from the data. Based on the Pr/Sm_{MUQ} ratios and Sr and Ga contents, a correlation is observed between Sr

Table 1. Abundances of REE+Y (in ppm) for samples from unit 4B (Musselwhite deposit).

	4B							
	E599655	E599656	E599661	E599668	E599669	E599670	E599671	E599672
La_{MUQ}	0.005	0.003	0.044	0.021	0.014	0.004	0.002	0.010
Ce_{MUQ}	0.006	0.003	0.037	0.028	0.020	0.004	0.003	0.006
Pr_{MUQ}	0.010	0.003	0.032	0.042	0.015	0.004	0.005	0.006
Nd_{MUQ}	0.022	0.002	0.033	0.070	0.021	0.003	0.007	0.006
Sm_{MUQ}	0.080	0.003	0.034	0.117	0.025	0.002	0.010	0.006
Eu_{MUQ}	0.428	0.014	0.096	0.442	0.071	0.008	0.033	0.022
Gd_{MUQ}	0.218	0.003	0.040	0.193	0.026	0.003	0.014	0.009
Tb_{MUQ}	0.243	0.007	0.039	0.214	0.025	0.004	0.015	0.010
Dy_{MUQ}	0.308	0.003	0.042	0.307	0.028	0.003	0.016	0.008
Y_{MUQ}	0.592	0.002	0.055	0.653	0.032	0.003	0.017	0.017
Ho_{MUQ}	0.354	0.006	0.044	0.414	0.028	0.004	0.018	0.012
Er_{MUQ}	0.422	0.003	0.049	0.592	0.032	0.004	0.019	0.011
Tm_{MUQ}	0.425	0.012	0.054	0.758	0.037	0.005	0.025	0.015
Yb_{MUQ}	0.485	0.003	0.050	1.039	0.039	0.006	0.030	0.009
Lu_{MUQ}	0.520	0.010	0.057	1.37	0.046	0.011	0.044	0.017
$(La/La^*)_{MUQ}$	2.334	0.242	1.478	1.386	1.850	0.990	0.800	1.831
$(Ce/Ce^*)_{MUQ}$	2.889	0.219	1.228	1.799	2.785	0.993	1.257	1.015
$(Pr/Pr^*)_{MUQ}$	0.721	1.562	0.914	0.865	0.715	0.957	0.980	0.997
$(Eu/Eu^*)_{MUQ}$	3.608	3.708	2.620	3.031	2.751	2.599	2.657	2.970
$(Gd/Gd^*)_{MUQ}$	1.273	0.521	1.048	1.085	1.022	0.724	1.048	0.983
$(Lu/Lu^*)_{MUQ}$	1.207	0.045	0.878	1.104	0.899	0.982	1.079	0.548
$(Pr/Yb)_{MUQ}$	0.021	1.029	0.640	0.041	0.382	0.565	0.162	0.613
$(Pr/Sm)_{MUQ}$	0.125	1.297	0.941	0.362	0.598	1.442	0.471	1.013
$(Nd/Yb)_{MUQ}$	0.044	0.561	0.659	0.068	0.543	0.521	0.217	0.618
Y/Ho	44.008	9.790	32.550	41.586	30.284	22.126	25.450	37.808
Eu/Sm	1.166	1.172	0.618	0.826	0.623	0.723	0.682	0.836
Sm/Yb	0.365	1.752	1.5	0.248	1.409	0.864	0.759	1.334
Th/U	0.103	0.116	0.261	0.496	0.216	1.127	0.256	0.621

and Ga contents for sample E5996551 that suggests the sample may be influenced by a Sr-, Ga-rich source (i.e. proxies of Ca and Al) (Fig. 5b, c). This source could be explained by presence of aluminum- and calcium-rich (actinolite) amphibole minerals in the chert around the line traverse that would also explain the difference in ∑REE contents for the samples; however, the low concentration of Ga and particularly Sr in the other samples could be due to analytical error. Therefore, this discrimination has to be used carefully.

Finally, the garnet-biotite schist (unit 4F) facies (Fig. 6) shows variable enrichment in the MREEs relative to both the HREEs and LREEs (Pr/ SmMUQ = 0.18–0.8) and only moderate positive Eu anomalies (Eu/Eu*MUQ = 1.08–1.94) (Table 3). This unit is distinguished from the other units by its REE+Y signature and, furthermore, is similar to the argillite studied by Thurston et al. (2011), which illustrated only weak hydrothermal influence. Based on Pr/Sm_{MUQ} ratios and the Sr and Ga contents (Fig. 6b, c), sample E599657 could be affected by the presence of garnet, which would explain the Ga:Sr ratios. The other samples show a strong correlation among Sr, Ga, and Ta content relative to Pr/Sm_{MUQ} ratios (Fig. 6b, c, d) that could be explained by the presence of plagioclase and biotite (e.g. Moran, 2008).

To define the environment of precipitation for the garnet-grunerite-(chert) (unit 4EA) and the garnet-biotite schist (unit 4F) facies, which only show the hydrothermal influence, the Th/U ratio is used. This ratio in epiclastic sedimentary rocks does not vary much and falls close to the Th/U ratio of average upper continental crust (i.e. 3.9; Bau and Alexander (2009)). Therefore, in river water draining continental areas the ratio will be close to 3.9 (or within a 15% error margin); whereas in seawater it will be closer to 1 if it is considered that the Archean seawater is anoxic (Fig. 7a); however, for the Musselwhite mine samples, all the data plot far from the

Table 2. Abundances of REE+Y (in ppm) for samples from unit 4EA (Musselwhite deposit).

	4EA							
	E599654	E599659	E599660	E599662	E599663	E599665	E599666	E599667
La_{MUQ}	0.015	0.013	0.005	0.004	0.001	0.001	0.001	0.209
Ce_{MUQ}	0.010	0.013	0.006	0.003	0.001	0.002	0.001	0.110
Pr_{MUQ}	0.009	0.008	0.009	0.003	0.002	0.002	0.002	0.108
Nd_{MUQ}	0.010	0.008	0.004	0.002	0.001	0.001	0.001	0.134
Sm_{MUQ}	0.009	0.007	0.006	0.002	0.002	0.001	0.002	0.142
Eu_{MUQ}	0.020	0.022	0.029	0.007	0.007	0.007	0.006	0.637
Gd_{MUQ}	0.008	0.006	0.008	0.003	0.003	0.001	0.003	0.214
Tb_{MUQ}	0.007	0.006	0.018	0.004	0.005	0.004	0.004	0.193
Dy_{MUQ}	0.007	0.005	0.009	0.002	0.002	0.002	0.002	0.225
Y_{MUQ}	0.008	0.006	0.010	0.000	0.001	0.001	0.003	0.506
Ho_{MUQ}	0.007	0.006	0.017	0.003	0.004	0.004	0.005	0.238
Er_{MUQ}	0.006	0.005	0.011	0.001	0.001	0.002	0.004	0.250
Tm_{MUQ}	0.005	0.008	0.034	0.005	0.008	0.01	0.010	0.212
Yb_{MUQ}	0.003	0.003	0.011	0.003	0.003	0.003	0.005	0.199
Lu_{MUQ}	0.006	0.007	0.029	0.006	0.008	0.007	0.010	0.217
$(La/La^*)_{MUQ}$	2.018	1.514	0.161	0.513	0.022	0.040	0.120	3.027
$(Ce/Ce^*)_{MUQ}$	1.406	1.448	0.170	0.306	0.042	0.052	0.274	1.594
$(Pr/Pr^*)_{MUQ}$	0.890	0.794	1.724	1.326	2.335	2.092	1.346	0.880
$(Eu/Eu^*)_{MUQ}$	2.339	3.194	3.111	2.194	2.103	3.488	2.546	3.971
$(Gd/Gd^*)_{MUQ}$	0.986	0.945	0.607	0.741	0.692	0.364	0.835	1.209
$(Lu/Lu^*)_{MUQ}$	1.327	0.368	0.094	0.072	0.018	0.023	0.136	1.415
$(Pr/Yb)_{MUQ}$	2.672	2.424	0.774	0.811	0.693	0.690	0.295	0.540
$(Pr/Sm)_{MUQ}$	1.042	1.240	1.385	1.145	0.979	2.026	0.954	0.757
$(Nd/Yb)_{MUQ}$	2.974	2.340	0.397	0.463	0.184	0.192	0.158	0.674
Y/Ho	31.205	29.859	15.962	3.621	4.338	4.113	16.522	55.910
Eu/Sm	0.508	0.713	1.015	0.616	0.610	1.235	0.811	0.978
Sm/Yb	5.664	4.319	1.233	1.566	1.566	0.752	0.682	1.574
Th/U	0.141	0.114	0.212	0.237	0.109	0.961	0.762	0.151

field for river water, hence it is suggested that the initial seawater signature expected in all the banded iron-formation units was completely overprinted or replaced due to the influence of a hydrothermal fluid either during or postdating diagenesis in these samples.

All of the banded iron-formation facies in the Musselwhite deposit area show a variable seawater component and positive Eu anomalies (Fig. 3a, 4a, 5a, 6a) that suggest that these samples have been influenced by both seawater and hydrothermal fluids. In order to evaluate the contribution of end-member seawater and hydrothermal fluids, a conservative mixing calculation was done (Fig. 8a) that indicates that a high-T hydrothermal fluid contribution of less than 20% is needed to produce the observed Eu/Sm ratios (Fig. 8a).

Meadowbank deposit

The data set from the Meadowbank area was reported and discussed by Gourcerol et al. (2014). The Far West, West IF, Central BIF, East BIF, and Grizzly were analyzed and normalized to MUQ (Fig. 9) and with some minor exceptions, seawater and hydrothermal inputs were observed in each deposit. The West banded iron-formation and East iron-formaton showed a detrital component, as indicated by relatively flat REE patterns, particularly for the LREEs. Using a conservative mixing calculation, an estimate of the detrital input is calculated for each sample using MUQ as a shale reference.

For the West iron-formation, sample AMB-128328 was used as an initial composition lacking any hydrogeneous input, which was then mixed incrementally with detritus. The detrital input has the effect of producing flatter REE patterns

Table 3. Abundances of REE+Y (in ppm) for samples from units 4E and 4F (Musselwhite deposit).

	4E		4F				
	E599651	E599652	E599653	E599657	E599658	E599664	E599673
La_{MUQ}	0.027	0.002	0.000	0.004	0.004	0.003	0.005
Ce_{MUQ}	0.020	0.002	0.001	0.005	0.009	0.004	0.007
Pr_{MUQ}	0.016	0.003	0.001	0.004	0.012	0.007	0.009
Nd_{MUQ}	0.016	0.002	0.000	0.004	0.020	0.007	0.010
Sm_{MUQ}	0.016	0.002	0.002	0.005	0.064	0.020	0.015
Eu_{MUQ}	0.045	0.009	0.004	0.013	0.047	0.032	0.015
Gd_{MUQ}	0.022	0.004	0.003	0.007	0.053	0.019	0.01
Tb_{MUQ}	0.022	0.006	0.004	0.008	0.018	0.015	0.011
Dy_{MUQ}	0.02	0.005	0.002	0.005	0.007	0.008	0.004
Y_{MUQ}	0.030	0.005	0.000	0.005	0.003	0.005	0.002
Ho_{MUQ}	0.024	0.006	0.004	0.006	0.003	0.009	0.008
Er_{MUQ}	0.025	0.006	0.002	0.006	0.002	0.005	0.002
Tm_{MUQ}	0.029	0.005	0.008	0.005	0.005	0.012	0.012
Yb_{MUQ}	0.023	0.006	0.003	0.003	0.003	0.003	0.003
Lu_{MUQ}	0.025	0.007	0.008	0.007	0.004	0.010	0.011
$(La/La^*)_{MUQ}$	1.646	0.710	0.024	0.842	0.970	0.631	0.659
$(Ce/Ce^*)_{MUQ}$	1.200	0.674	0.062	0.878	2.105	0.832	0.922
$(Pr/Pr^*)_{MUQ}$	0.900	1.146	2.212	1.018	0.825	1.121	1.066
$(Eu/Eu^*)_{MUQ}$	2.425	2.595	1.503	1.942	1.084	1.672	1.068
$(Gd/Gd^*)_{MUQ}$	1.059	0.920	0.796	0.904	1.818	1.097	0.775
$(Lu/Lu^*)_{MUQ}$	0.607	1.407	0.099	1.386	0.157	0.151	0.038
$(Pr/Yb)_{MUQ}$	0.707	0.435	0.368	1.280	3.449	1.958	2.735
$(Pr/Sm)_{MUQ}$	1.006	1.075	0.520	0.832	0.183	0.326	0.632
$(Nd/Yb)_{MUQ}$	0.696	0.385	0.121	1.170	5.769	2.178	2.925
Y/Ho	32.8	25.714	2.545	20.424	22.558	15.175	7.983
Eu/Sm	0.617	0.797	0.406	0.523	0.162	0.34	0.223
Sm/Yb	1.551	0.894	1.566	3.398	41.593	13.274	9.558
Th/U	0.176	0.372	0.261	0.237	0.109	0.154	0.961

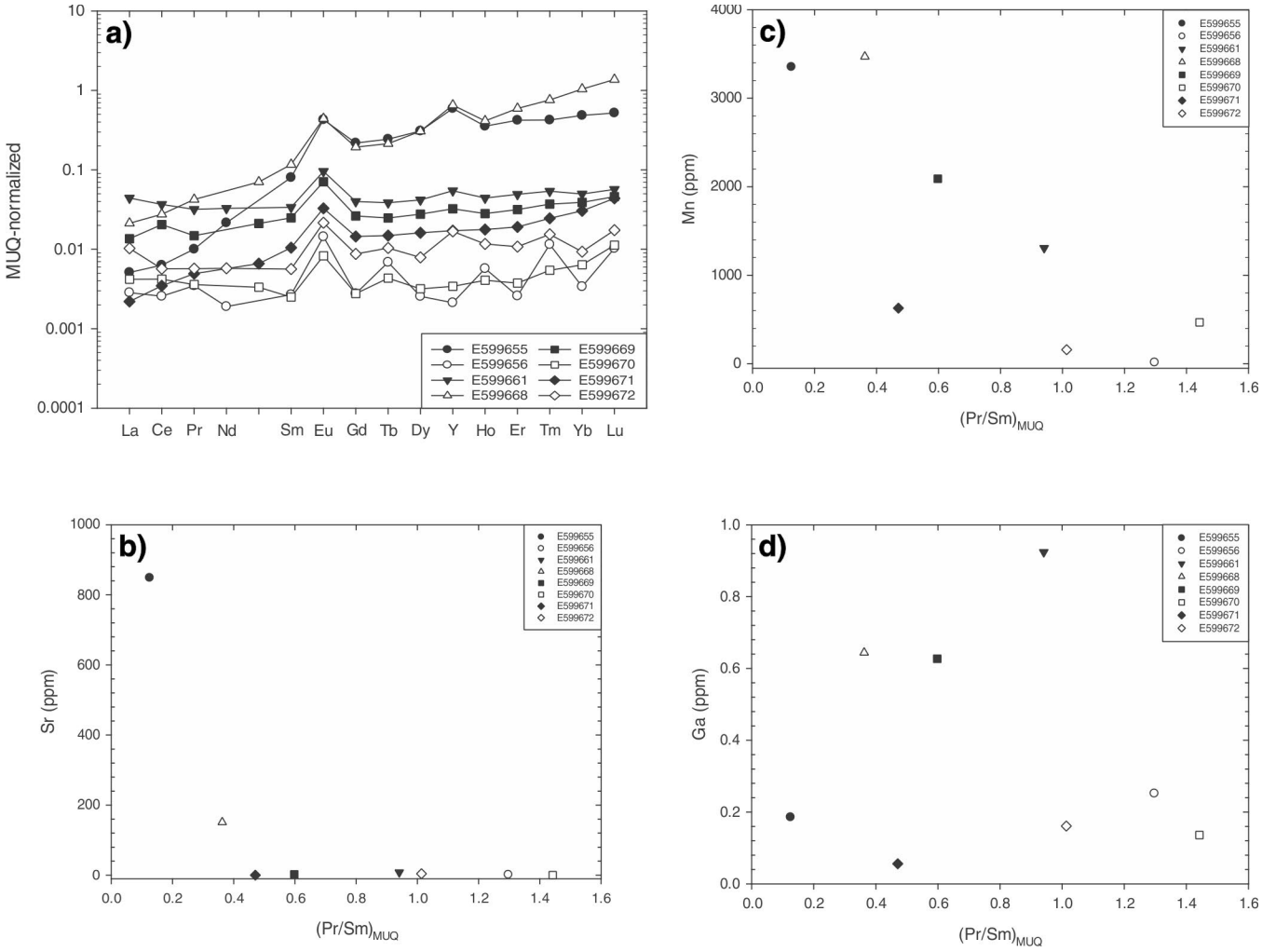

Figure 3. Plots of geochemical data for chert samples from the 4B unit at Musselwhite deposit area; **a)** shale (MUQ) -normalized REE patterns reflecting the influence of ambient seawater and hydrothermal fluids, **b)** Sr versus $(Pr/Sm)_{MUQ}$, **c)** Mn versus $(Pr/Sm)_{MUQ}$, and **d)** Ga versus $(Pr/Sm)_{MUQ}$.

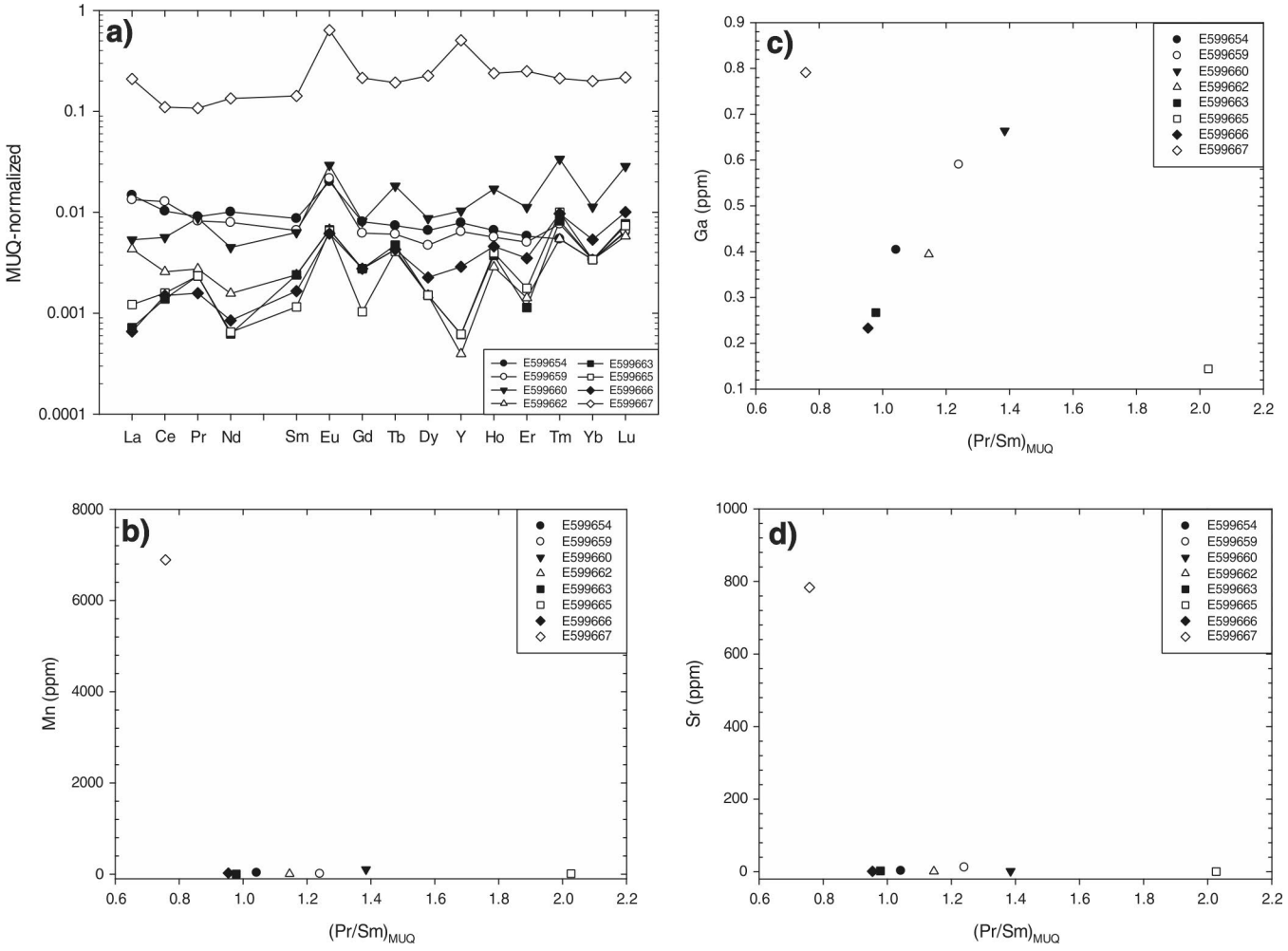

Figure 4. Geochemical data for chert samples from the 4EA unit at Musselwhite deposit area; **a)** shale (MUQ) -normalized REE patterns reflecting the influence of ambient seawater and hydrothermal fluids, **b)** Mn versus $(Pr/Sm)_{MUQ}$, **c)** Ga versus $(Pr/Sm)_{MUQ}$, **d)** Sr versus $(Pr/Sm)_{MUQ}$.

commencing with 0.1% contaminant (Fig. 10a). The contamination is very efficient at modifying the primary REE pattern and therefore, can account for most of the patterns observed for samples from this area. The mixing calculations suggest that the majority of samples were affected by less than 5% shale contamination (Fig. 10b).

For the East banded iron-formation, sample AMB-126246 is used as the initial composition to assess contamination. In this case, contamination with shale does not appear to account for the REE patterns as well as observed for the West iron-formation (Fig. 10c) as only four samples (i.e. AMB-126245, AMB-126247, AMB-126248, AMB-126250) are located on or close to the mixing trend (Fig. 10d). Thus it appears that samples from the West iron-formation have been more affected than the East banded iron-formation by shale contamination, as constrained by the composition used for the mixing calculations.

For the samples of Meadowbank deposit area, the Th/U versus $(Ce/Ce^*)_{MUQ}$ diagram is used to further test the importance of seawater (Fig. 7b). The data confirm the dominance of seawater, as suggested previously using the positive La, Gd, Y anomalies and enrichment in HREEs relative to MREEs and LREEs. The samples from the West banded iron-formation show a larger dispersion relative to the other Meadowbank deposit data and, even more so to that observed for the Musselwhite mine samples. This dispersion of data may be produced by the more extensive shale contamination postulated for the Meadowbank banded iron-formation. This is supported by the conservative mixing calculations shown in Figure 8b that indicate that a high-T hydrothermal fluid contribution of higher than 20% is adequate to explain the Eu/Sm ratios.

SUMMARY AND DISCUSSION

The trace-element signatures for chert in Algoma-type banded iron-formation units from two gold deposit settings have been determined in order to: 1) constrain the origin of the banded iron-formation units, 2) assess the effect of superimposed hydrothermal processes possibly related to gold mineralization on the chert; and 3) assess the consequent implications for banded iron-formation–hosted gold deposits in general. This report represents the second part of this study (Gourcerol et al., 2014). Importantly, in this phase

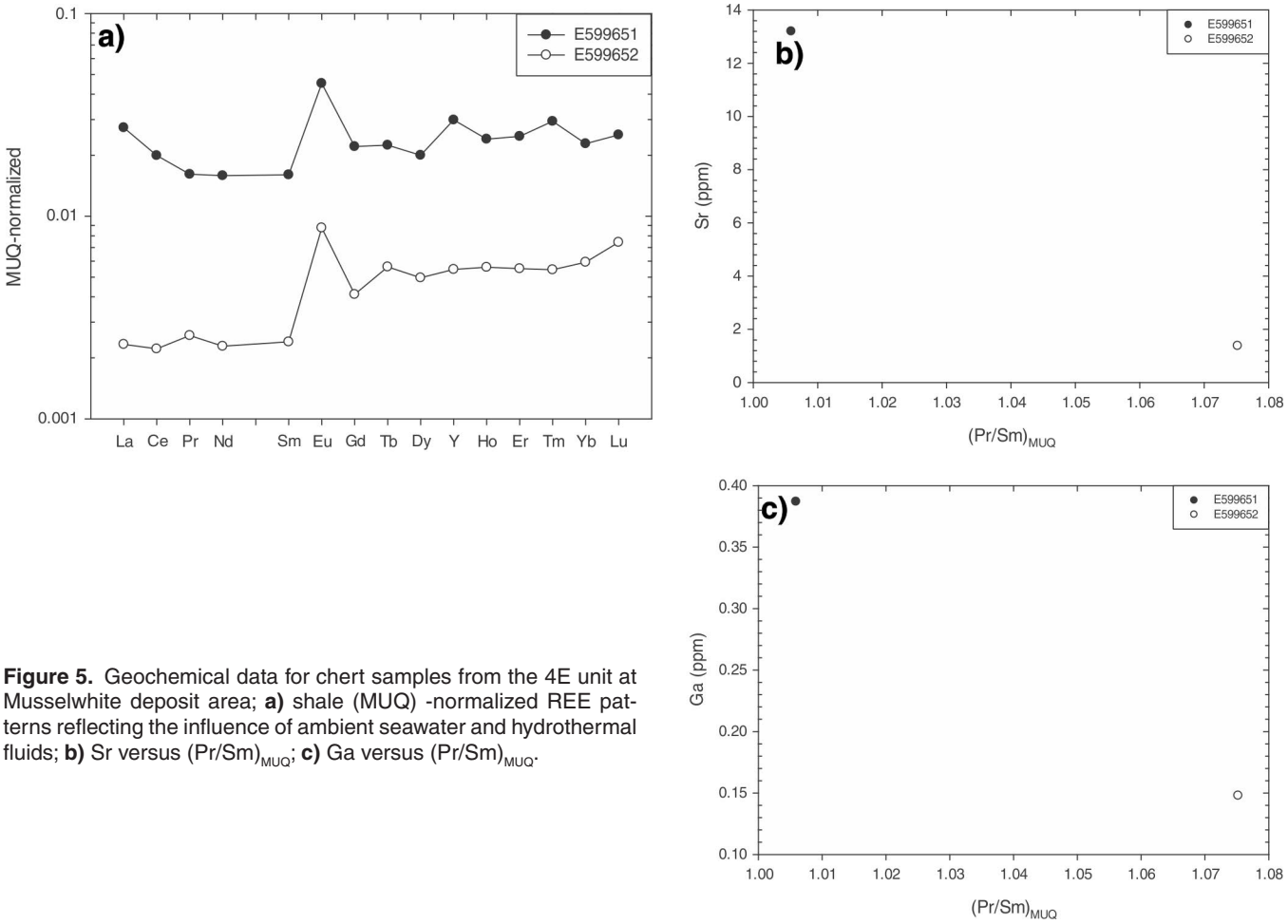

Figure 5. Geochemical data for chert samples from the 4E unit at Musselwhite deposit area; **a)** shale (MUQ) -normalized REE patterns reflecting the influence of ambient seawater and hydrothermal fluids; **b)** Sr versus $(Pr/Sm)_{MUQ}$; **c)** Ga versus $(Pr/Sm)_{MUQ}$.

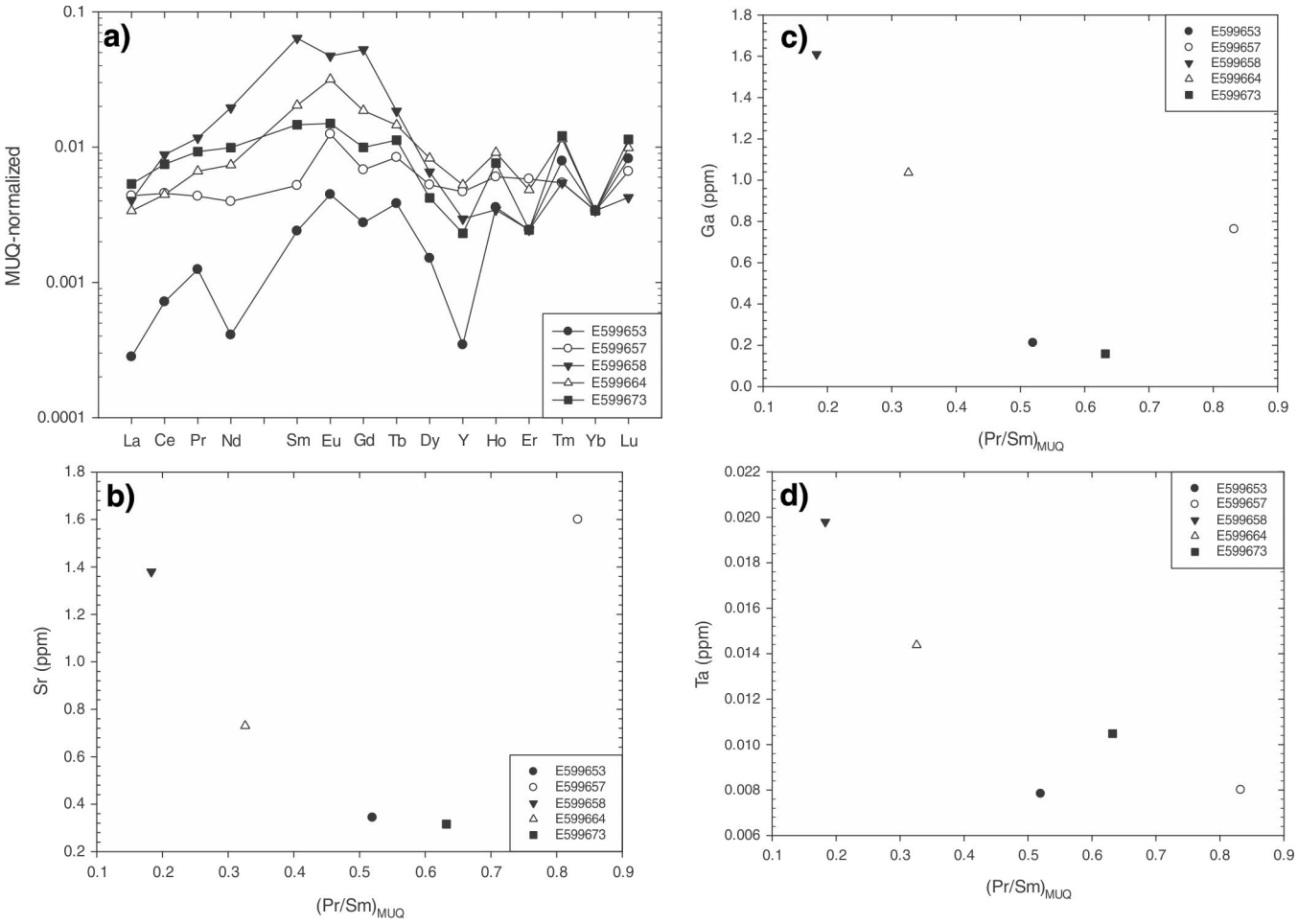

Figure 6. Geochemical data for chert samples from the 4F unit at Musselwhite deposit area; **a)** shale (MUQ)-normalized REE patterns reflecting the influence of ambient seawater and hydrothermal fluids; **b)** Sr versus $(Pr/Sm)_{MUQ}$; **c)** Ga versus $(Pr/Sm)_{MUQ}$; **d)** Ta versus $(Pr/Sm)_{MUQ}$.

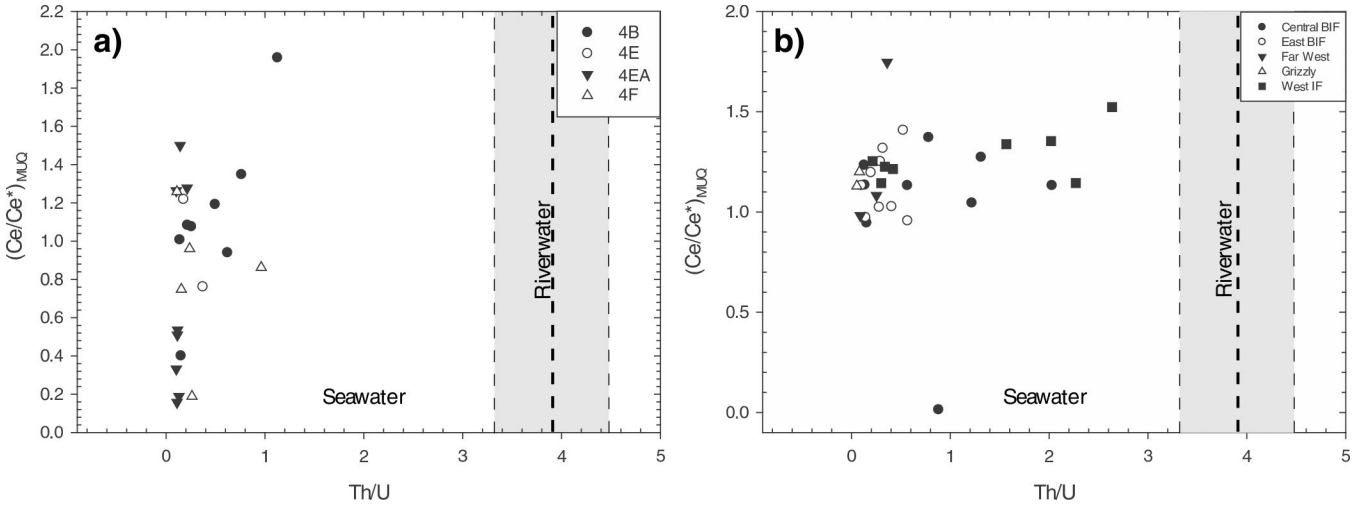

Figure 7. Plots of Th/U versus $(Ce/Ce^*)_{MUQ}$ for samples from **a)** Musselwhite, and **b)** Meadowbank deposits compared to the fields for river water and seawater based on the continental crust Th/U value of 3.9. A margin of errors of 15% is applied here (*after* Bau and Alexander, 2009).

of the study the present authors validated the application of using LA ICP-MS analysis in traverse mode on carefully selected chert bands within banded iron-formation units with the appropriate analytical protocols to provide quantitatively meaningful data. It was also shown that these data, when plotted in MUQ-normalized patterns, provided internally consistent patterns that reflect the nature and origin of the fluids from which the chert precipitated. The consistency of the patterns noted in this study indicates that potentially primary chemical signatures have been retained within the selected chert samples despite the fact that several postformation deformation and metamorphic events, in some cases to amphibolite facies, have affected the rocks.

Implications for the depositional processes of banded iron-formation units

Although the Musselwhite and Meadowbank deposits differ by their petrographic features, style of gold mineralization, and geological tectonic setting, the chert samples show similar geochemistry and depositional setting:

1) A seawater component is recognized in most of the banded iron-formation units, as reflected by enrichment in the HREEs relative to LREEs and MREEs, and positive La, Gd, Y anomalies. In some banded iron-formation units (e.g. 4EA, 4F), the combination of the Th/U ratios and Eu/Eu* values suggest that a hydrothermal component overprinted or replaced the seawater component either during or after diagenesis and thus likely during mineralizing processes;
2) A hydrothermal contribution is recognized in all the banded iron-formation units as reflected in positive Eu anomalies. This hydrothermal component is estimated at 0.1% to 30%, using the trace-element chemistry of black-smoker fluids as an end member, thus confirming that banded iron-formation units formed in areas where black-smoker systems formed part of the geological setting.
3) A detrital contribution is observable in all the banded iron-formation units either as a trace contaminant or observable volcanic detritus, depending on the proportion of detritus involved. The shale contamination appears, however, to be more significant in the data for samples from the West iron-formation and East banded iron-formation.

The results of this study indicate that Algoma-type banded iron-formation units were formed in a marine setting close to discharge zones for hydrothermal fluids (here, black-smoker–type fluids).

Implications for the gold mineralization

A significant outcome of this phase of the study is the recognition of a possible chemical overprinting by hydrothermal fluids on the chert bands close to gold mineralized

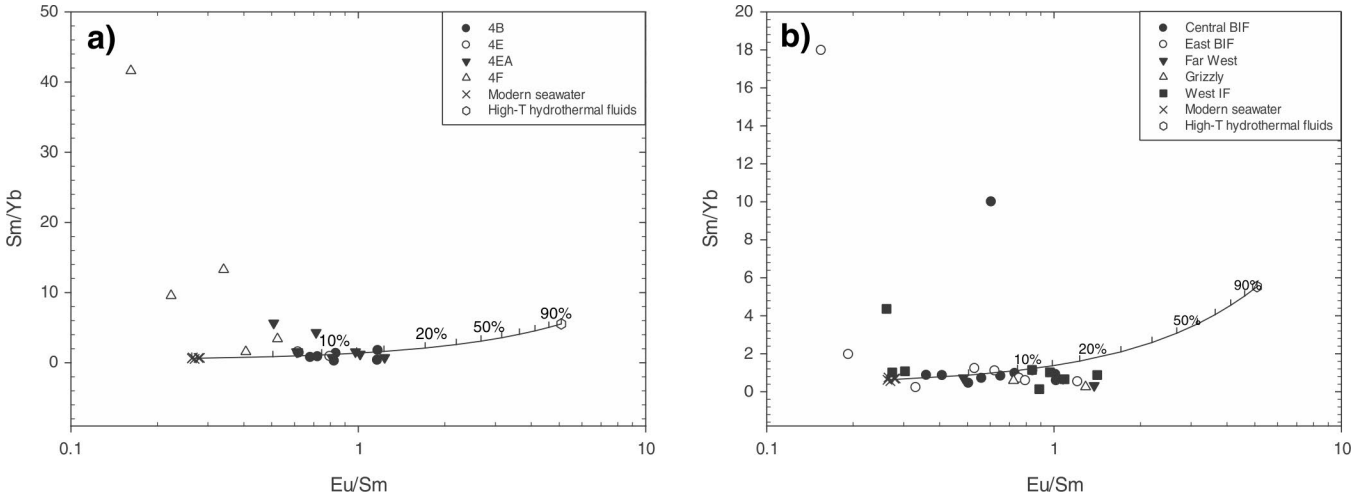

Figure 8. Plots of elemental ratio data (Eu/Sm and Sm/Yb) for samples from **a)** Musselwhite and **b)** Meadowbank deposits that are used to assess potential contamination of samples with a high-T hydrothermal fluid, as illustrated with the two-component conservative mixing lines. The data for the black-smoker fluid is from Bau and Dulski (1999) and data for seawater is from Alibo and Nozaki (1999).

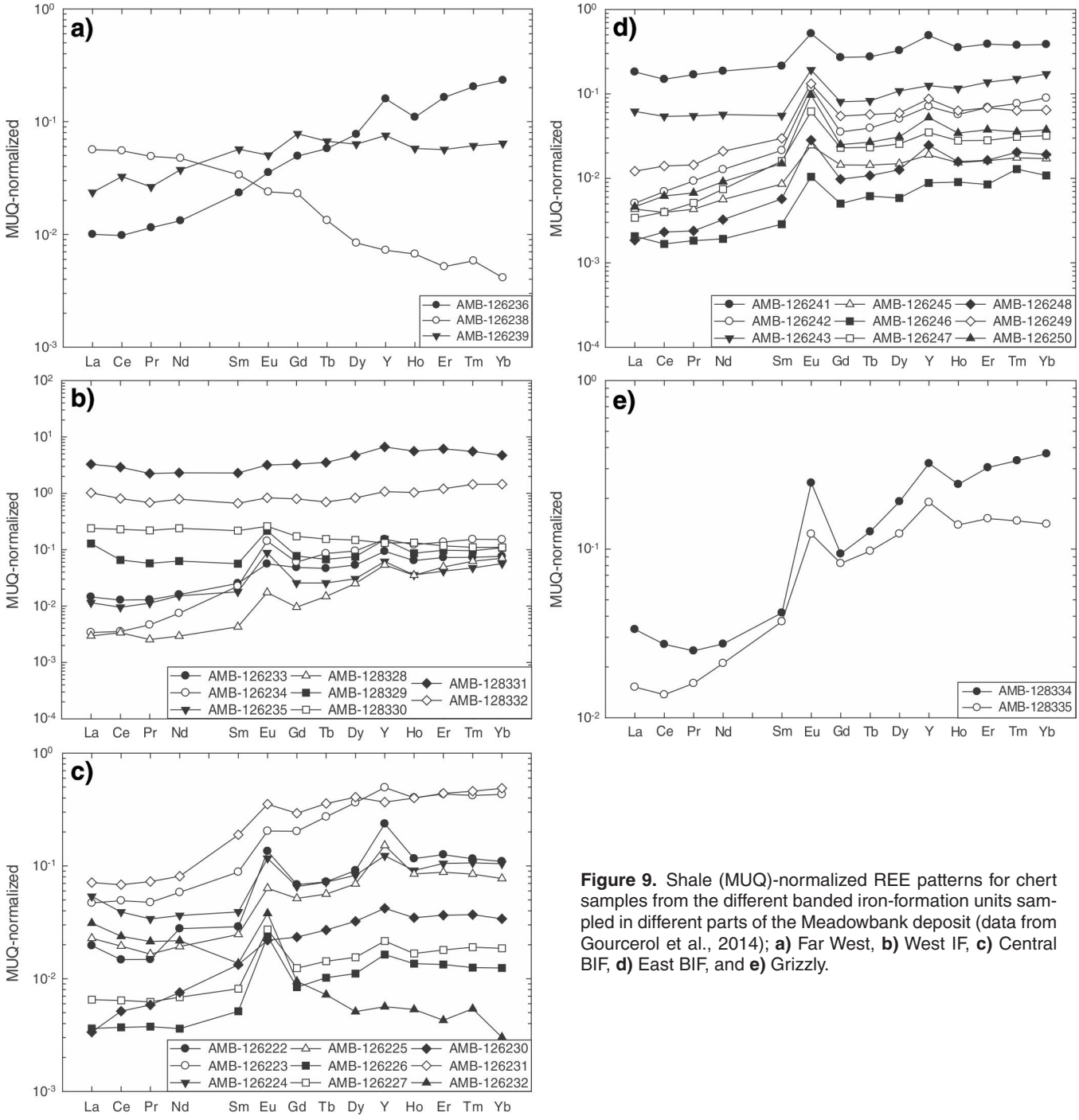

Figure 9. Shale (MUQ)-normalized REE patterns for chert samples from the different banded iron-formation units sampled in different parts of the Meadowbank deposit (data from Gourcerol et al., 2014); **a)** Far West, **b)** West IF, **c)** Central BIF, **d)** East BIF, and **e)** Grizzly.

zones, as recorded by the modification of the original seawater-type REE+Y patterns. At the Musselwhite deposit, this possible overprint is illustrated by the 4EA and 4F units. Although unit 4F is largely a metamorphosed argillite and is not strictly considered as a banded iron-formation (i.e. as chemical sedimentary rocks composed of iron-rich mineral interlayered with chert bands, but more as an iron-formation (22.7% Fe_2O_3, n = 70)), it still is inferred to show the influence of an overprinting hydrothermal fluid. Unit 4EA, a banded iron-formation, shows strong Eu anomalies that coincide with negative Ce anomalies ($(Ce/Ce^*)_{MUQ}$ = 0.04–1.59, average = 0.66, standard deviation at 1.13), which should be close to 1 in Archean seawater (i.e. anoxic conditions). This unit also represents the more mineralized banded iron-formation facies in the Musselwhite deposit area.

ACKNOWLEDGMENTS

The authors gratefully acknowledge the staff of Agnico Eagle Mines Ltd. and Goldcorp Ltd. and more particularly the Meadowbank and Musselwhite regional exploration crews. The authors also thank S. Pehrsson, O. Côté-Mantha, and J. Biczok for discussions regarding the regional geological setting of the study areas. Finally, the authors sincerely acknowledge the contribution of B. Dubé of the Geological Survey of Canada for initiating the TGI-4 Lode-Gold Project and for his input and continued support. The study is supported by both TGI-4 funding from Natural Resources Canada and funding through a Natural Sciences and Engineering Research Council Collaborative Research and Development agreement with participation by Agnico Eagle Mines Ltd. and Goldcorp.

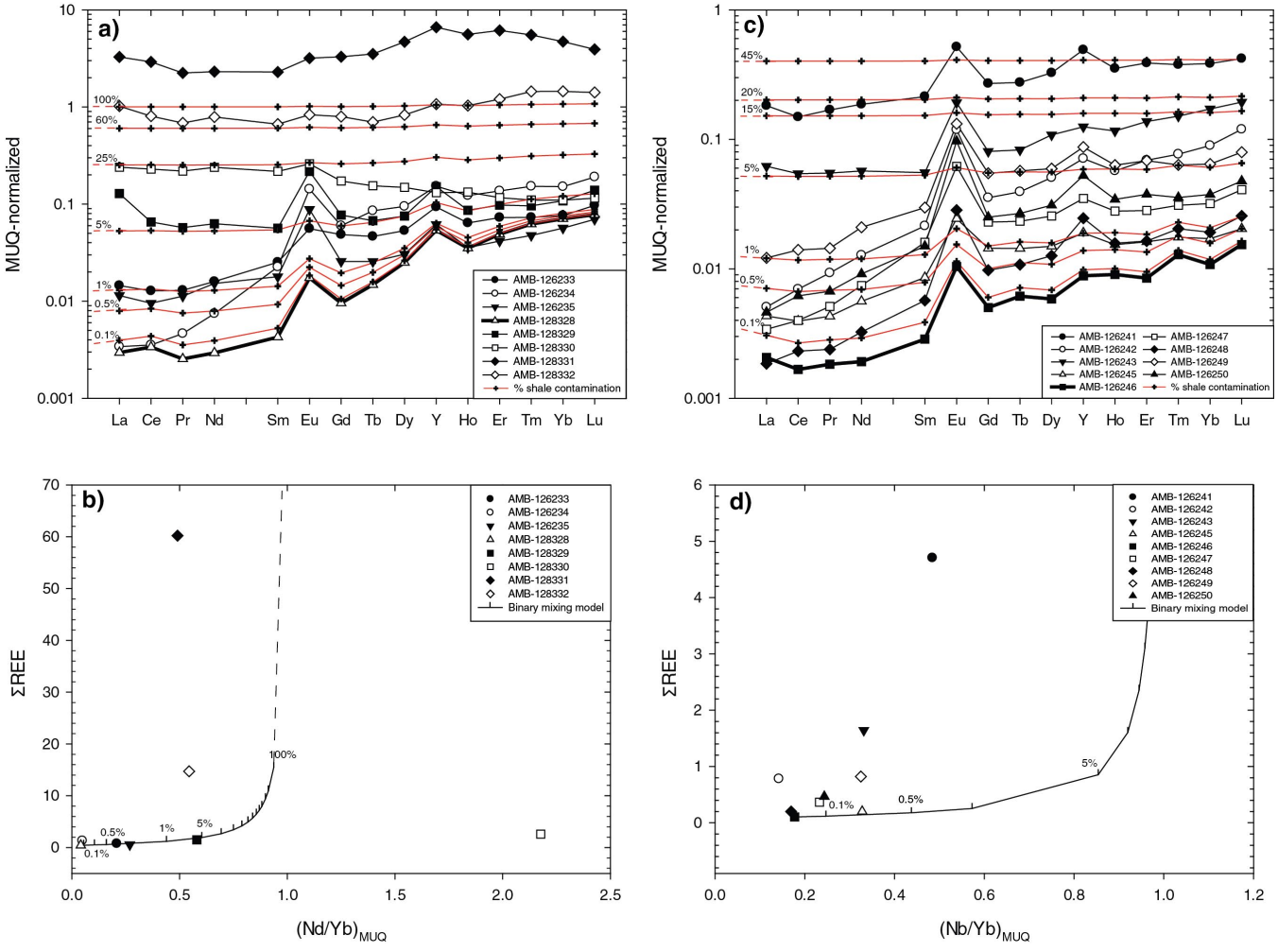

Figure 10. Geochemical data for chert samples from the **a)** West IF and **b)** East BIF at the Meadowbank deposit compared to variable amounts of shale contamination (red lines) using sample AMB-128328 as the initial sample without any contamination. A plot of $(Nd/Yb)_{MUQ}$ versus ∑REE content (ppm) of samples from the **c)** West BIF and **d)** East BIF in the Meadowbank area. Except for three of the eight samples, all are close to or on the mixing line and suggest up to 5% shale contamination.

REFERENCES

Alexander, B.W., Bau, M., Andersson, P., and Dulski, P., 2008. Continentally-derived solutes in shallow Archean sea water; rare earth element and Nd isotope evidence in iron formation from the 2.9 Ga Pongola Supergroup, South Africa; Geochimica et Cosmochimica Acta, v. 72, p. 378–394. doi:10.1016/j.gca.2007.10.028

Alibo, D.S. and Nozaki, Y., 1999. Rare earth elements in seawater: particle association, shale-normalization, and Ce oxidation; Geochimica et Cosmochimica Acta, v. 63, p. 363–372. doi:10.1016/S0016-7037(98)00279-8

Allwood, A.C., Kamber, B.S., Walter, M.R., Burch, I.W., and Kanik, I., 2010. Trace element record depositional history of an Early Archean stromatolitic carbonate platform; Chemical Geology, v. 270, p. 148–163. doi:10.1016/j.chemgeo.2009.11.013

Armitage, A.E., James, R.S., and Goff, S.P., 1996. Gold mineralization in Archean banded iron formation, Third Portage Lake area, Northwest Territories, Canada; Exploration and Mining Geology, v. 5, no. 1, p. 1–15.

Ashton, K.E., 1985. Archean orthoquartzites from the Churchill Structural Province near Baker Lake, N.W.T.; Geological Association of Canada–Mineralogical Association of Canada; Program with Abstracts, Geological Association of Canada, Fredericton, New Brunswick, May 15–17, 1985, v. 10, p. A2.

Aspler, L.B. and Chiarenzelli, J.R., 1996. Stratigraphy, sedimentology and physical volcanology of the Henik Group, central Ennadai-Rankin greenstone belt, Northwest Territories, Canada: Late Archean paleogeography of the Hearne Province and tectonic implications; Precambrian Research, v. 77, p. 59–89. doi:10.1016/0301-9268(95)00045-3

Bau, M. and Alexander, B.W., 2009. Distribution of high field strength elements (Y, Zr, REE, Hf, Ta, Th, U) in adjacent magnetite and chert bands and in reference standards FeR-3 and FeR-4 from the Temagami iron-formation, Canada, and the redox level of the Neoarchean ocean; Precambrian Research, v. 174, p. 337–346. doi:10.1016/j.precamres.2009.08.007

Bau, M. and Dulski, P., 1996. Distribution of Y and rare-earth elements in the Penge and Kuruman Iron Formations, Transvaal Supergroup, South Africa; Precambrian Research, v. 79, p. 37–55. doi:10.1016/0301-9268(95)00087-9

Bau, M. and Dulski, P., 1999. Comparing yttrium and rare earths in hydrothermal fluids from the Mid-Atlantic Ridge: implications for Y and REE behaviour during near-vent mixing and for the Y/Ho ratio of Proterozoic seawater; Chemical Geology, v. 155, p. 77–90. doi:10.1016/S0009-2541(98)00142-9

Bekker, A., Slack, J.F., Planavsky, N., Krapez, B., Hofmann, A., Konhauser, K.O., and Rouxel, J., 2010. Iron formation: the sedimentary product of a complex interplay among mantle, tectonic, oceanic and biospheric processes; Economic Geology and the Bulletin of the Society of Economic Geologists, v. 105, p. 467–508. doi:10.2113/gsecongeo.105.3.467

Biczok, J., Hollings, P., Klipfel, P., Heaman, L., Maas, R., Hamilton, M., Kamo, S., and Friedman, R., 2012. Geochronology of the North Caribou greenstone belt, Superior Province Canada: implications for tectonic history and gold mineralization at the Musselwhite mine; Precambrian Research, v. 192–195, p. 209–230. doi:10.1016/j.precamres.2011.10.012

Bleeker, W., 2007. The Slave Craton: Geological and Metallogenic Evolution; *in* Mineral Deposits of Canada: A Synthesis of Major Deposit-types, District Metallogeny, the Evolution of Geological Provinces, and Exploration Methods, (ed.) W.D. Goodfellow; Geological Association of Canada, Mineral Deposits Division, Special Publication no. 5, p. 849–879.

Bolhar, R., Van Kranendonk, M.J., and Kamber, B.S., 2005. A trace element study of siderite-jasper banded iron formation in the 3.45 Ga Warrawoona Group, Pilbara craton-Formation from hydrothermal fluids and shallow seawater; Precambrian Research, v. 137, p. 93–114. doi:10.1016/j.precamres.2005.02.001

Breaks, F.W., Osmani, I.A., and DeKemp, E.A., 2001. Geology of the North Caribou Lake area, northwestern Ontario; Ontario Geological Survey, Open File Report 6023, 80 p.

Danielson, A., Moeller, P., and Dulski, P., 1992. The europium anomalies in banded iron formations and the thermal history of the oceanic crust; Chemical Geology, v. 97, p. 89–100. doi:10.1016/0009-2541(92)90137-T

Davis, W.J. and Zaleski, E., 1998. Geochronological investigations of the Woodburn Lake group, Western Churchill province, Northwest Territories: preliminary results; *in* Radiogenic Age and Isotopic Studies: Report 11; Geological Survey of Canada, Current Research 1998-F, p. 89–97.

DeKemp, E.A., 1987. Stratigraphy, provenance, and geochronology of Archean supracrustal rocks of western Eyapamikama Lake area, Northwestern Ontario; M.Sc. thesis, Carleton University, Ottawa, Ontario, 98 p.

Goldfarb, R.J., Groves, D.I., and Gardoll, S., 2001. Orogenic gold and geologic time: a global synthesis; Ore Geology Reviews, v. 18, p. 1–75. doi:10.1016/S0169-1368(01)00016-6

Goldfarb, R.J., Baker, T., Dubé, B., Groves, D.I., Hart, C.J.R., and Gosselin, P., 2005. Distribution, character and genesis of gold deposits in metamorphic terranes; *in* Economic Geology 100th Anniversary Volume, (ed.) J.W. Hedenquist, J.F.H. Thompson, R.J. Goldfarb, and J.P. Richards; p. 407–450.

Goodwin, A.M., 1973. Archean iron-formations and tectonic basins of the Canadian Shield; Economic Geology and the Bulletin of the Society of Economic Geologists, v. 68, p. 915–933. doi:10.2113/gsecongeo.68.7.915

Gourcerol, B., Thurston, P.C., Kontak, D.J., and Côté-Mantha, O., 2014. Interpretations and implications of preliminary LA ICP-MS analysis of chert for the origin of geochemical signatures in banded iron-formations (BIFs) from the Meadowbank gold deposit, Western Churchill Province, Nunavut; Geological Survey of Canada, Current Research 2014-1, 26 p. doi:10.4095/293129

Hall, R.S. and Rigg, D.M., 1986. Geology of the West Anticline Zone, Musselwhite Prospect, Opapimiskan Lake, Ontario, Canada; *in* Gold '86; an International Symposium on the Geology of Gold Deposits, (ed.) A.J. Macdonald; proceedings volume; GOLD '86, Toronto, Ontario, p. 124–136.

Hanor, J.S. and Duchac, K.C., 1990. Isovolumetric silicification of early Archean komatiites; geochemical mass balances and constraints on origin; The Journal of Geology, v. 98, p. 863–877. doi:10.1086/629458

Henderson, J.R., Henderson, M.N., Pryer, L.L., and Cresswell, R.G., 1991. Geology of the Whitehills-Tehek area, District of Keewatin: an Archean supracrustal belt with iron-formation hosted gold mineralization in the central Churchill Province; *in* Current Research, Part C; Geological Survey of Canada, Paper 91-1C, p. 149–156.

Hoffman, P.F., 1989. Precambrian geology and tectonic history of North America; *in* The Geology of North America — An Overview; (ed.) A.W. Bally and A.R. Palmer; Geological Society of America, The Geology of North America, Part A, p. 447–512.

Hollings, P. and Kerrich, R., 1999. Trace element systematics of ultramafic and mafic volcanic rocks from the 3 Ga North Caribou greenstone belt, northwestern Superior Province; Precambrian Research, v. 93, p. 257–279. doi:10.1016/S0301-9268(98)00088-6

Hrabi, R.B., Barclay, W.A., Fleming, D., and Alexander, R.B., 2003. Structural evolution of the Woodburn Lake group in the area of the Meadowbank gold deposit, Nunavut, Geological Survey of Canada, Current Research 2003-C27, 10 p. doi:10.4095/214396

Isaac, C., 2008. Stable isotope (N, O, H) geochemistry, petrology and compositions of biotite of the Musselwhite Mine, Ontario: implications for mineralization; M.Sc. thesis, Lakehead University, Thunder Bay, Ontario, 104 p.

James, H.L., 1954. Sedimentary facies iron-formation; Economic Geology and the Bulletin of the Society of Economic Geologists, v. 49, p. 235–293. doi:10.2113/gsecongeo.49.3.235

Janvier, V., Castonguay, S., Mercier-Langevin, P., Dubé, B., McNicoll, V., Malo, M., Pehrsson, S., and Bécu, V., 2013. Recognizing optimum banded-iron formation hosted gold environments in ancient, deformed and metamorphosed terranes: Preliminary results from the Meadowbank deposit, Nunavut; Geological Survey of Canada, Open File 7407, 1 sheet. doi:10.4095/292589

Kamber, B.S. and Webb, G.E., 2007. Transition metal abundances in microbial carbonate: a pilot study based on in situ LA-ICP-MS analysis; Geobiology, v. 5, p. 375–389. doi:10.1111/j.1472-4669.2007.00129.x

Kamber, B.S., Bolhar, R., and Webb, G.E., 2004. Geochemistry of late Archean stromatolites from Zimbabwe: evidence for microbial life in restricted epicontinental seas; Precambrian Research, v. 132, p. 379–399. doi:10.1016/j.precamres.2004.03.006

Kerswill, J.A., 1993. Models for iron-formation-hosted gold deposits; *in* Mineral Deposit Modelling, (ed.) R.V. Kirkham, W.D. Sinclair, R.I. Thorpe, and J.M. Duke; Geological Association of Canada, Special Paper 40, p. 171–199.

Kerswill, J.A., 1996. Iron-formation-hosted stratabound gold; Chapter 15 *in* Geology of Canadian Mineral Deposit Types, (ed.) O.R. Eckstrand, W.D. Sinclair, and R.I. Thorpe; Geological Survey of Canada, Geology of Canada, no. 8, p. 367–382 (*also* Geological Society of Amercia, The Geology of North America, v. P-1).

Kolb, M.J., 2010. A microstructural study of Musselwhite mine and Hammond reef shear-zone-hosted gold deposits; M.Sc. thesis, Lakehead University, Thunder Bay, Ontario, 197 p.

Lawrence, M.G. and Kamber, B.S., 2006. The behavior of the rare earth elements during estuarine mixing- revisited; Marine Chemistry, v. 100, p. 147–161. doi:10.1016/j.marchem.2005.11.007

McNicoll, V., Dubé, B., Biczok, J., Castonguay, S., Oswald, W., Mercier-Langevin, P., Skulski, T., and Malo, M., 2013. The Musselwhite gold deposit, North Caribou greenstone belt, Ontario: new high-precision U-Pb ages and their impact on the geological and structural setting of the deposit; Abstract, Geological Association of Canada–Mineralogical Association of Canada, annual meeting, Winnipeg, Manitoba, May 24, 2013.

Miller, A.R. and Tella, S., 1995. Stratigraphic settings of semi-conformable alteration in the Spi Lake area, Kaminak greenstone belt, Churchill Province, Northwest Territories; Geological Survey of Canada, Current Research 1995-C, p. 175–186.

Moran, P., 2008. Lithogeochemistry of the sedimentary stratigraphy and metasomatic alteration in the Musselwhite gold deposit, North Caribou Lake metavolcanic-metasedimentary belt, Superior Province, Canada: implications for deposition and mineralization; M.Sc. thesis, Lakehead University, Thunder Bay, Ontario, 351 p.

Oswald, W., Dubé, B., Castonguay, S., McNicoll, V., Biczok, J., Mercier-Langevin, P., Malo, M., and Skulski, T., 2014. New insights on the structural and geological setting of the world-class Musselwhite gold deposit, Superior Province, northwestern Ontario; Geological Survey of Canada, Open File 7633, 1 sheet. doi:10.4095/294817

Otto, A., 2002. Ore forming processes in the BIF-hosted gold deposit Musselwhite Mine, Ontario, Canada; M.Sc. thesis, Freiberg Institute of Mining and Technology, Freiberg, Germany, 86 p.

Pehrsson, S.J. and Wilkinson, L., 2004. Geology, Meadowbank gold deposit area, Nunavut; Geological Survey of Canada, Open File 4269, scale 1:20 000. doi:10.4095/215550

Pehrsson, S., Wilkinson, L., Zaleski, E., Kerswill, J., and Alexander, R.B., 2000. Structural geometry of the Meadowbank deposit area, Woodburn Lake group—implications for a major gold deposit in the western Churchill province; *in* Geo-Canada 2000—The Millennium Geoscience Summit CD-ROM, Calgary, Alberta, May 29–June 1, 2000, 1 CD-ROM.

Pehrsson, S.J., Berman, R.G., and Davis, W.J., 2013. Paleoproterozoic orogenesis during Nuna aggregation: a case study of reworking of the Rae craton, Woodburn Lake, Nunavut; Precambrian Research, v. 232, p. 167–188.

Percival, J.A., 2007. Geology and metallogeny of the Superior Province, Canada; *in* Mineral Deposits of Canada: A Synthesis of Major Deposit-Types, District Metallogeny, the Evolution of Geological Provinces, and Exploration Methods, (ed.) W.D. Goodfellow; Geological Association of Canada, Special Publication No. 5, Mineral Deposits Division, p. 903–928.

Phillips, G.N., Groves, D.I., and Martyn, J.E., 1984. An epigenetic origin for Archean banded iron-formation-hosted gold deposits; Economic Geology and the Bulletin of the Society of Economic Geologists, v. 79, p. 162–171. doi:10.2113/gsecongeo.79.1.162

Planavsky, N., Bekker, A., Rouxel, O.J., Kamber, B.S., Hofmann, A.W., Knudsen, A., and Lyons, T.W., 2010. Rare earth element and yttrium compositions of Archean and Paleoproterozoic Fe formations revisited: new perspectives on the significance and mechanisms of deposition; Geochimica et Cosmochimica Acta, v. 74, p. 6387–6405. doi:10.1016/j.gca.2010.07.021

Roddick, J.C., Henderson, J.R., and Chapman, H.J., 1992. U-Pb ages from the Archean Whitehills-Tehek Lakes Supracrustal Bell, Churchill Province, District of Keewatin, Northwest Territories; *in* Radiogenic Age and Isotopic Studies: Report 6; Geological Survey of Canada, Paper 1992-2, p. 31–40.

Schau, M., 1982. Geology of the Prince Albert Group in parts of Walker Lake and Laughland Lake map areas, District of Keewatin; Geological Survey of Canada, Bulletin 337, 62 p. doi:10.4095/109249

Sherlock, R.L., Alexander, R.B., March, R., and Barclay, W.A., 2001a. Geologic setting of the Meadowbank iron formation-hosted gold deposits; Geological Survey of Canada, Current Research 2001-C11, 23 p. doi:10.4095/212081

Sherlock, R.L., March, R., and Kellner, A.R., 2001b. Geology of the Meadowbank iron formation-hosted gold deposit; Geological Survey of Canada, Open File 3149, 1 sheet, doi:10.4095/212961

Sherlock, R.L., Pehrsson, M.S., Logan, A.V., Hrabi, R.B., and Davis, W.J., 2004. Geological Setting of the Meadowbank Gold Deposits, Woodburn Lake Group, Nunavut; Exploration and Mining Geology, v. 13, no. 1–4, p. 67–107. doi:10.2113/gsemg.13.1-4.67

Stott, G.M., Corfu, F., Breaks, F.W., and Thurston, P.C., 1989. Multiple orogenesis in northwestern Superior Province; Geological Association of Canada; Abstracts, v. 14, p. A56.

Thurston, P., Osmani, I., and Stone, D., 1991. Northwestern Superior Province: review and terrane analysis; *in* Geology of Ontario, (ed.) P.C. Thurston, H.R. Williams, R.H. Sutcliffe, and G.M. Stott; Ontario Geological Survey; Special Volume 4, pt. 1, p. 80–142.

Thurston, P.C., Kamber, B.S., and Whitehouse, M., 2011. Archean cherts in banded iron formation: insight into Neoarchean ocean chemistry and depositional processes; Precambrian Research, v. 214–215, p. 227–257.

Geological Survey of Canada Project 340331NU61